# Detection of Wake-Sleep Transitions
# with Prototype Vector-Based Neural Networks

## David Sommer, Martin Golz

University of Applied Sciences of Schmalkalden
Department of Computer Science
P.O. Box 182; D-98574 Schmalkalden; Germany
{sommer, golz}@informatik.fh-schmalkalden.de

## Abstract

*Electrophysiological and eyetracking signals of eleven subjects recorded in overnight driving simulations were analyzed using three different neural networks: learning vector quantization, self-organizing maps and growing cell structures. In the first investigation the electrophysiological signals were screened for slow eye movements (SEM), a typical pattern of wake-sleep transitions. To characterize the electroencephalogram (EEG) of such transitions, the spectral power densities of the simultaneously recorded EEG were analyzed and subsequently clustered without the common summation in spectral bands. Any knowledge about the number of clusters didn't exist. Several hierarchical agglomerative clustering procedures, the winner histogram and the unified distance matrix (U-matrix) of self-organizing maps did not provide a consistent estimate of the number of clusters. After applying a modified watershed transform to the U-matrix, a stable count of nine different clusters was obtained. The proposed method works automatically and is not restricted to two-dimensional maps. The subsequent investigations concerned discrimination between eyetracking signals immediately before wake-sleep transitions and during awake phases. Among many training runs for several types of neural networks and for several training parameters, test-set classification rates of about 80% were obtained for the LVQ3 algorithm, processing spectral power densities of pupil diameter only.*

## 1 Introduction

Driving a car overnight is simultaneously a continuous tracking task and a low-event-rate vigilance task. As a result of normal fatigue, performance in both tasks deteriorates over time and can lead to hazardous situations. The proportion of lethal accidents caused by short sleep events at the steering wheel has been estimated as being up to 10% [1, 2]. The EEG as a functional measure of brain activity has been investigated by several authors; for a review see Santamaria & Chiappa [3]. They report a great deal of variability in the EEG of drowsiness among different subjects. Among others, Kuhlo and Lehmann [4] report the slowing of the EEG frequency content, mainly slowing alpha (7.5 … 12.5 Hz) rhythms, until the disappearance of alpha and the appearance of theta (3.5 … 7.5 Hz) rhythms. In a large normative study with 200 male subjects 24-35 years old, the EEG of drowsiness was found to have a considerably more complex and variable pattern than in the awake state [5]. In all subjects they registered pendular, horizontal eye movements with a period time of 3…4 sec, so-called slow eye movements (SEM).

Our first investigations were focused on these SEM and the correlated spectral characteristic of the EEG. In a recent paper, correlations between fast irregular eye movements and EEG segments with peak values in the alpha and beta band were reported [6], but correlations between SEM and EEG measures were not reported.

Our subsequent investigations were done to explore characteristics of eyetracking signals immediately before the onset of a wake-sleep transition. The measurement of pupil size dynamic and eye movements to estimate a subject's alertness level has been suggested by many research groups [6-10]. The first three groups used electro-oculography (EOG); the later two groups used infrared corneal reflection as the measurement principle. Our intention is to discriminate eye-tracking signals of wake-sleep transitions from those of awake states.

## 2 Material

Eleven subjects (3 females, 8 males) aged between 19 and 36 years participated in an overnight driving simulator study. Their task was intentionally monotonous, simply to avoid major lane deviations. One driving session of 25 min length was carried out every hour from 1 a.m. to 7 a.m. EEG was filtered with a 30 Hz lowpass filter and recorded in two unipolar and two bipolar recordings (C3-A2, C4-A1, O1-C3, O2-C4), as were

EOG (oblique) and ECG, and digitized at a rate of 64 samples per second. Afterwards, the EEG during a SEM event was segmented to a length of 2 sec. SEMs were automatically detected using the cross correlation function between the EOG signal and a sine-signal. The frequency and the amplitude of the sine-signal were estimated by fitting the sine-signal to 15 SEM signals from three subjects obtained through visual scoring.

The eyetracker worked in the near infrared with an accuracy of 0.65 deg and measured the pupil diameter (D) and the horizontal (X) and vertical (Y) component of the eye gaze point in the plane of the driving simulator screen with a sampling rate of 30 Hz. The X- and Y-signals had a series of missing values during eye blinks. They were substituted for by Beziér spline interpolation. Outlier elimination was also necessary, especially for the Y-signal immediately after an eye blink. The X-, Y- and D-signals immediately before wake-sleep transitions were segmented to a length of 8 sec.

Before applying the discrete Fourier transform, any linear trends in the EEG and eyetracking segments were eliminated and a Welch window was applied to reduce bias effects due to nonstationarity and sidelobe effects. Additionally, the Welch method of averaging the periodogram over shifted windows was used, enabling a reduction of variance by a factor of $n^{-1}$ (n being the number of shifted windows).

# 3 Clustering of EEG Segments

The input vectors for the subsequent analysis consisted of 47 spectral components (2 to 25 Hz; 0.5 Hz steps). A principal component analysis (PCA) was routinely computed, but there was no reason to assume input vectors in a linear subspace because the last ten principal components had a residual variance of about 8%. A Scree test and the Kaiser criteria for the covariance matrix (number of eigenvalues greater than one) indicated 13 principal components, but they explained only 30% of the total variance.

Five different hierarchical agglomerative clustering procedures yielded an inconsistent estimation of the numbers of clusters, depending on the method, on the termination measure and on the standardization of the data [11]. Seven clusters were suggested by the centroid method, and six clusters were found by the Ward method. The model underlying all measures for terminating the agglomerative process is too simple. Agglomerative clustering methods are incapable of finding an optimal solution for non-compact clusters.

The self-organizing map (SOM) [12] is a prototype vector-based neural network method to perform cluster analysis. Using the principle of competitive learning, the prototype vectors adapt to the probability density function of the input vectors. The similarity between the input vector **x** and the prototype vector **w** was calculated using Euclidian distance. During training an arbitrary prototype vector $\mathbf{w}_j$ is updated at iteration index t by:

$$\Delta\mathbf{w}_j(t) = \eta(t)\, h_{cj}(t)\, [\mathbf{x}(t) - \mathbf{w}_j(t)] \qquad (\mathbf{1})$$

Where $\eta(t)$ is a learning rate factor decreasing during training and $h_{cj}(t)$ is a neighborhood function between the prototype vector $\mathbf{w}_j$ and $\mathbf{w}_c$, the prototype vector winning the competition. The neighborhood function $h_{cj}(t)$ also decreases during training. The neighborhood relationships are defined by a topological structure and are fixed during training. We used a two-dimensional rectangular relationship. In the final phase of training, the fine-adjustment phase [13], the neighborhood radius is very small, leading to updates of the winning prototype vectors $\mathbf{w}_c$ and of their nearest neighbors.
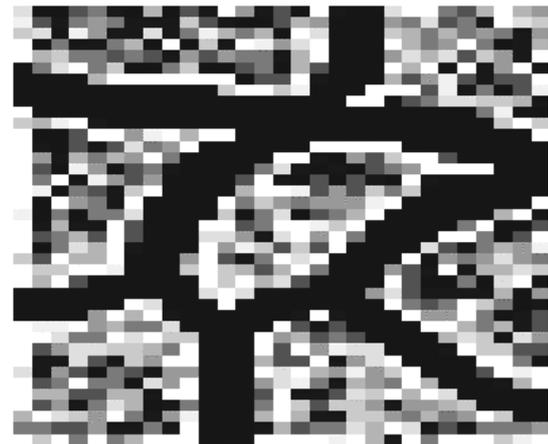


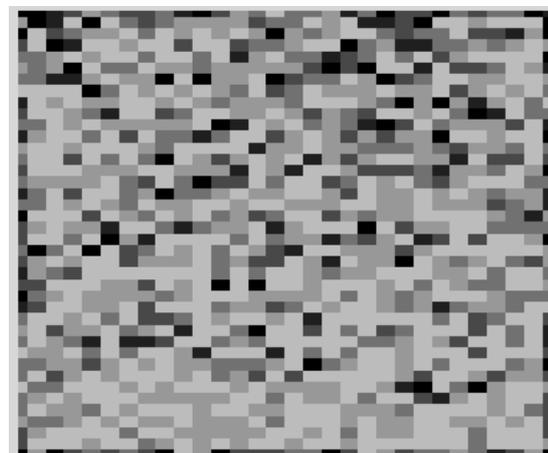Figure 1: Relative winner frequency for a SOM with 30x40 neurons for Gaussian mixture data



Figure 2: Relative winner frequency for a SOM with 30x40 neurons for SEM-EEG data

In the case of one-dimensional topological structures, it can be shown analytically [13] that training rule (Eq.1) leads to an approximation of a monotonous function of the probability density function of the input vectors. Two-dimensional topologies result in a compromise between density approximation and minimization of mean squared error of vector quantization [14].

For existing compact regions of input vectors and existing density centers, as for Gaussian mixtures, the evaluation of the relative winner frequency of the prototypes led to a visualization of clusters. Figure 1 shows such a gray-level-coded winner histogram. Seven areas with increased winner frequency are evident.

The Gaussian mixture data were generated by defining seven cluster centers and seven covariance matrices and adding normal distributed noise in a 47-dimensional space, as in our experimental data set. The estimated total covariance matrix of the generated data set and of the experimental data set was nearly the same.

The black-colored units in Figure 1 are never-winning neurons (dead neurons), which make it easy to distinguish clusters. For the experimental data set, a distinction of regions with increased winner frequency is not possible.
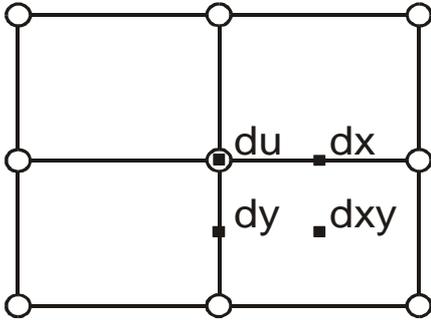


Figure 3: Definition of the U-matrix and localization on the rectangular topological structure, shown for the neuron in the center only. Circles: positions of neurons; black squares: positions of U-matrix elements

But the SOM contains considerable additional information. For example, the distance between topological neighboring prototype vectors in the feature space can be computed. In the case of topology preservation, these prototype vectors remain neighbors also in the output space (the two-dimensional map) [15]. If the distance between two neighboring prototypes is small, then they probably represent one cluster. Otherwise they probably represent different clusters. The visualization of the distances between neighboring prototype vectors was introduced as the unified distance matrix

(U-matrix) [16]. In a two-dimensional rectangular topology, the U-matrix is calculated in $n_X$ columns and $n_Y$ rows.

For every prototype vector $\mathbf{w}_{x,y}$, where $x$ and $y$ are the indices of the topological structure, the Euclidian distances $dx$ and $dy$ between two neighbors and the distance $dxy$ to the next but one neighbor is calculated:

$$dx(x,y) = \left\| \mathbf{w}_{x,y} - \mathbf{w}_{x+1,y} \right\| \qquad (2)$$

$$dy(x,y) = \left\| \mathbf{w}_{x,y} - \mathbf{w}_{x,y+1} \right\| \qquad (3)$$

$$dxy(x,y) = \frac{1}{2} \left( \frac{\left\| \mathbf{w}_{x,y} - \mathbf{w}_{x+1,y+1} \right\|}{\sqrt{2}} + \frac{\left\| \mathbf{w}_{x,y+1} - \mathbf{w}_{x+1,y} \right\|}{\sqrt{2}} \right) \qquad (4)$$

$$\mathbf{U} = \begin{bmatrix} du(1,1) & dx(1,1) & du(2,1) & \ldots & du(n_x,1) \\ dy(1,1) & dxy(1,1) & dy(2,1) & \ldots & dy(n_x,1) \\ du(1,2) & dx(1,2) & du(2,2) & \ldots & du(n_x,2) \\ dy(1,2) & dxy(1,2) & dy(2,2) & \ldots & dy(n_x,2) \\ \vdots & \vdots & \vdots & \ddots & \vdots \\ du(1,n_y) & dx(1,n_y) & du(2,n_y) & \ldots & du(n_x,n_y) \end{bmatrix} \qquad (5)$$

The distance $du$ is calculated using the mean over eight surrounding distances. With four distances for each neuron $dx$, $dy$, $dxy$ and $du$ (Figure 3), the $(2n_X - 1)$ x $(2n_Y - 1)$ U-matrix is well defined.

The U-matrix elements were mapped on a gray scale. Light gray levels indicate low values, and dark gray-levels indicate high values.
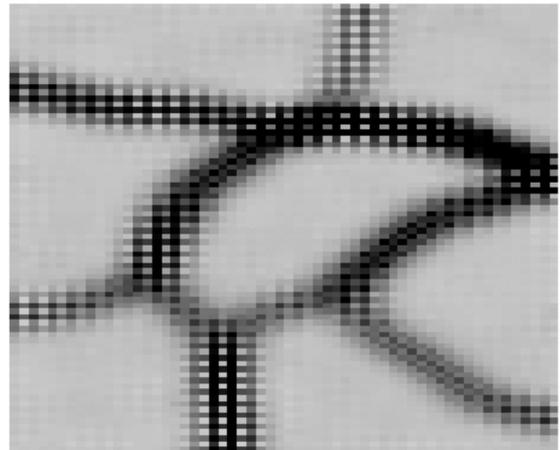


Figure 4: U-matrix for SOM from Figure 1

Scoring the U-matrix of Gaussian mixture data (Figure 4) leads visually to seven clusters. As expected, the cluster regions on the map are regions

of small distances between the prototype vectors, which are separated by small regions of large distances. The U-matrix of the SEM-EEG data (Figure 9) has much more complexity. It is difficult to determine borders.
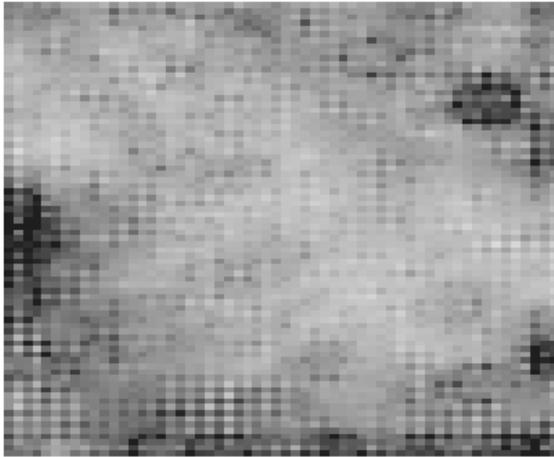


Figure 5: U-matrix for SOM from Figure 2

Costa et al. [17] propose an automatic segmentation of the U-matrix using the watershed algorithm of gray scale image processing. Regarding high values as mountains and low values as valleys, the algorithm can be illustrated by flooding the valleys with water; watersheds will be built up where the water converges. This algorithm leads to closed borders. It's not difficult to evaluate the number of clusters. All prototype vectors in one segmented region represent one cluster, and the fusion of their Voronoi sets leads to all items of a cluster.

It is difficult to choose suitable initial values for each reservoir; otherwise a generation of many segments is unavoidable [17]. The number of segments can be reduced during initialization by the threshold parameter $h_{min}$. All values which are lower than $h_{min}$ are assigned to the same value as $h_{min}$.

The results of segmentation are dependent on the size of the SOM. With a relatively large number of prototype vectors, many clusters are obtained. Smoothing the gray level function with a two-dimensional filter reduces the risk of multiple segmentations. The size of the SOM was considerably restricted when the topographic product [18] was taken into account. The topographic product is a measure for the correspondence of input and output space dimensions. We obtained an optimal value for a SOM size of 4 x 6, but the segmentation of the U-matrix failed for such small maps. Therefore we extended the size but retained the ratio of approximately 70%. On the other hand, it was shown that the topographic product was a

good measure for approximately linear manifolds only [15].

In several regions of the U-matrix (Figure 4, 5) black-and-white textures are observable. They describe relatively large differences between dx and dy and are connected with local stretchings of the SOM along one topological coordinate.

If the dx elements of the U-matrix, for example, are visualized only, some segment borders disappear. Up to now the following defaults were used:

- use of function du(x,y)
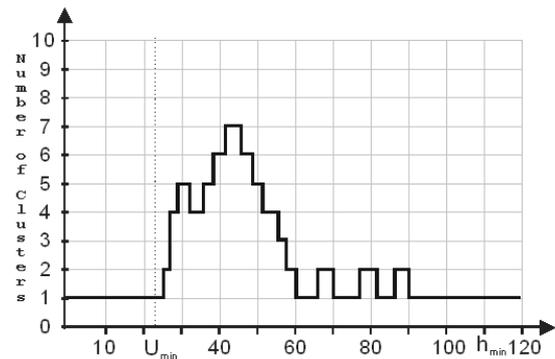- 3x3-Gaussian filtering
- watershed transformation



Figure 6: Number of clusters vs. $h_{min}$ for the U-matrix of Figure 5 without generation of new regions [7]
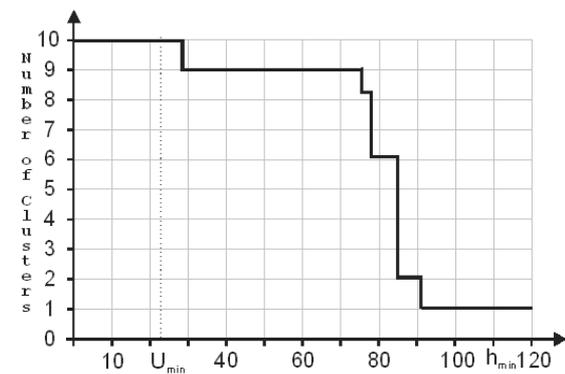


Figure 7: Number of clusters vs. $h_{min}$ for the U-matrix of Figure 5 with generation of new regions

The segmentation was repeated many times with increasing threshold parameter $h_{min}$ [17] (Figure 6). No plateau in the number of clusters was detectable. Therefore we propose a modification allowing the generation of new minima regions during flooding. For the most extended plateau, we obtained 9 clusters (Figure 7).

The segmentation of the SOM in 9 clusters is shown in Figure 8. The segments contain different numbers of prototype vectors. The fusion of their Voronoi sets, mentioned above, leads to the clusters (Figure 9). Cluster 2 and 7 contain input vectors with large magnitudes in the alpha1 band (7.5-10.5 Hz), cluster 9 in the alpha2 band (10.5-12.5 Hz), cluster 3 in the theta band (3.5-7.5 Hz) and cluster 5 in the delta band (1.0-3.5 Hz). In contrast to the usual summation in frequency bands, more details are available. The input vectors of cluster 2 and 7, for example, are large in the same spectral band, but they differ in the magnitude range and differ in other spectral bands.
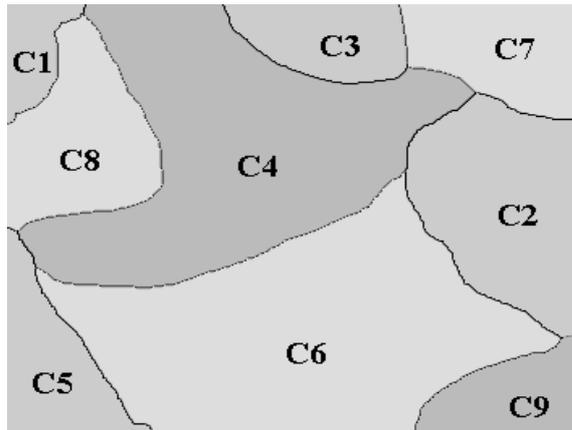


Figure 8: U-matrix from Figure 7 after watershed transformation

From Figure 9 one has the visual impression of homogeneous clusters, with the exception of clusters 1 and 4.
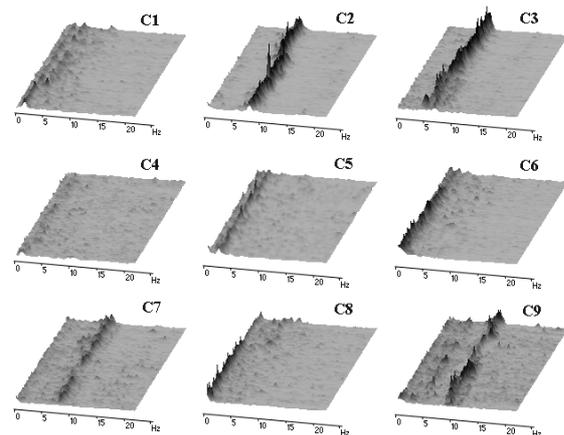


Figure 9: All 1652 input vectors grouped in 9 different clusters; horizontal = frequency, vertical = item, gray scale = spectral power density

An advantage of the described method is the relatively low number of free parameters and the ability to reproduce the results. A comprehensive validation of the results remains to be carried out.

# 4 Discrimination of Eyetracking Signals

We applied three types of prototype vector-based neural networks: the Learning Vector Quantization network (LVQ) [13], Self-Organizing Maps (SOM) [12] and Growing Cell Structures (GCS) [14]. LVQ is a network with supervised learning; here the binary information as to whether a wake-sleep transition is immanent was used as teaching input. Kohonen suggested three modifications: LVQ1, LVQ2 (LVQ2.1) and LVQ3. The first modification uses an adapted step size, whereas LVQ2 leads to an adaptation of neurons in interclass regions. LVQ3 additionally allows a slight adaptation of weight vectors in intraclass regions.

GCS networks were trained unsupervised, like SOM. After training, both network types were calibrated with the binary teaching input. GCS are incremental neural networks and with some restrictions are able to approximate the probability density function of the input vectors. The topological structure is a k-simplex. We chose k=1 and k=2 to be able to visualize. For SOM networks we used one- and two-dimensional rectangular topologies.

Each network was trained with several parameter settings and with several initializations of the weight vectors. Before each training, the learning set was randomly partitioned in training set (80%) and in test set (20%). After training had finished, the reclassification rate was estimated by the ratio of correctly classified to all applied input vectors of the training set. The classification rate was estimated in the same way with input vectors taken from the test set.

Calculations of classification and reclassification rates were done in $1.7 \cdot 10^6$ different network simulations with different parameter settings, like number of neurons, learning rate factor and parameters of the neighborhood function and different variables selections for the input vectors and different learning set partitions.

The optimal number of neurons ranged between 8 and 20. With an increasing number of neurons, the LVQ network shows better adaptation to the training set. The reclassification rate is mostly above 90%, but it shows a decreasing ability to generalize, as indicated by decreasing classification rates.

The average maximum classification rate was obtained by searching the maximum of the mean + standard deviation (upper curve in Figure 10) for all different settings of the LVQ networks (Table 1). The initialization with median assigned to

each component of the weight vectors the median value of this component over all input vectors. During data-driven initialization, each weight vector was assigned to a randomly selected input vector. Furthermore, in the first 30% of all training iterations, the network was trained disregarding the class membership of an input vector to diminish the variance of the classification rate described elsewhere [19].
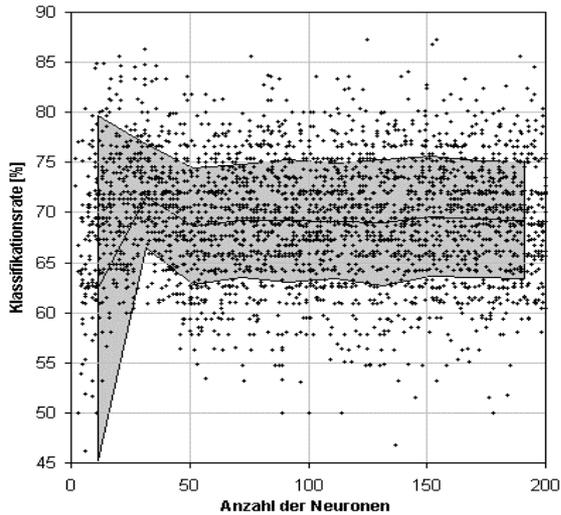


Figure 10: Test-set classification rate (in percent) vs. number of neurons for an LVQ3 network. The input vectors contain spectral power densities of the pupil diameter D only. The lines indicate the mean ± standard deviation range.

| Network | init | scaling | D | Y | X | DX | DXY |
|---------|------|---------|-----|-----|-----|-----|-----|
| LVQ1 | MED | --- | 77 | 69 | 70 | 71 | 72 |
| LVQ1 | DAT | --- | 77 | 68 | 71 | 70 | 71 |
| LVQ1 | DAT | SQR | 76 | | 71 | 72 | |
| LVQ1 | DAT | NRM | 75 | | 72 | 75 | |
| LVQ2 | MED | --- | 77 | | 75 | 74 | |
| LVQ2 | DAT | --- | 79 | | 75 | 74 | |
| LVQ3 | MED | --- | 80 | | 75 | 74 | |
| LVQ3 | DAT | --- | 80 | | 75 | 75 | |
| LVQ3 | DAT | SQR | 77 | | 73 | 74 | |
| LVQ3 | DAT | NRM | 73 | | 75 | 79 | |

Table 1: Average maximum test-set classification rate (in percent) with different LVQ networks, different initializations and different scaling applied to different feature sets (for details see text)

We tried a number of different scalings, but we want to report only the results of no scaling (---), the square root of each input vector component and the normalization of each component with respect to the sum of all components (relative value). In the columns "D", "Y", "X", the input vectors consisted only of the spectral power densities of the D, Y and X signal respectively. In column "DX" all spectral values of the D and X signal, and in "DXY" all spectral values of the D, X and Y signal were used. The best results were obtained with the set of input vectors obtained from the D signal only. Apparently, if we add further components to the input vectors as in the columns "XD" and "XYD", the results are not improvable. On the one hand we presented supplementary and independent information to the neural networks, but on the other hand the number of dimensions of the input space was obviously too great.

A typically calibrated SOM is shown in Figure 11. Large distances of neighbored weight vectors are visualized as gray shades using the U-matrix [16]. The input vectors of the awake state are mapped to the left lower part of the map, whereas the input vectors of the wake-sleep transitions (microsleep) are mapped to the right upper region. The prototype vectors representing the awake state have larger distances visualized by darker shades. Under the assumption that the SOM has found a correct approximation of the probability density function of the input vectors, this indicates that the microsleep class has a higher density and is more compact.
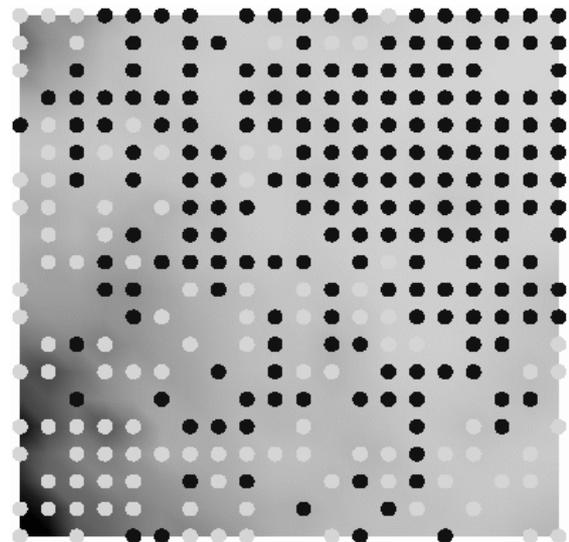


Figure 11: Typical calibrated SOM. Gray shades indicate the U-matrix. Microsleep events (dark nodes) and awake states (light nodes) are separable with some limitations. Vacancies indicate dead neurons.

The differentiated U-matrix (Figure 12) roughly shows the region of overlapping classes with light shades. The two classes are distributed in only two more or less compact and overlapping regions in the input space. This could explain the decreasing ability of generalization with increasing number of neurons and the onset of this effect at small numbers of neurons already.
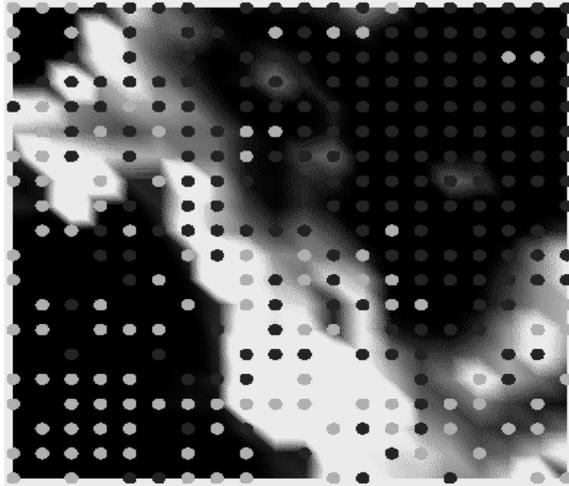


Figure 12: The same SOM with a differentiated U-matrix. Microsleep events (dark nodes) and awake states (light nodes) are separable with some limitations. Vacancies indicating dead neurons.

| network | no. of neur. | dim. | criter. | D | X | DX |
|---------|-------------|------|---------|-----|-----|-----|
| SOM | 20 x 1 | 1 | | 76 | 72 | 70 |
| SOM | 20 x 10 | 2 | | 74 | 68 | 68 |
| SOM | 20 x 20 | 2 | | 72 | 66 | 67 |
| GCS | 300 | 1 | PDF | 74 | 74 | 70 |
| GCS | 300 | 1 | VQE | 75 | 69 | 69 |
| GCS | 300 | 2 | PDF | 74 | 69 | 69 |
| GCS | 300 | 2 | VQE | 74 | 68 | 68 |

Table 2: Average maximum test-set classification rate (in percent) with SOM and GCS networks, different number of neurons applied to different feature sets (for details see text)

GCS networks were trained and tested with the same method as SOM. Additionally, there is a fast learning by inserting and deleting neurons depending on a local criterion. Two criteria were proposed [14]: the mean vector quantization error (vqe) and the local probability density function (pdf). For the calculation of the pdf, the volume of the n-dimensional voronoi cell was approximated with the volume of the n-dimensional hypercube, generated with the mean local weight vector distance [14].

Both networks, SOM and GCS, came to lower average maximum classification rates (Table 2). This is not surprising because their training is unsupervised.

With SOM and with GCS, the best results were obtained processing D data only and mapping on one-dimensional topology. In this case, it is not significant whether vqe or pdf is chosen as fast learning criterion function. When pdf and one-dimensional topology were chosen, the results were about equal for signal D and for X.

The visualization of the topology yielded no results. Between one and three separate topological nets grew during training. No net contained a large majority of input vectors of the microsleep class.

## 5 Conclusions

Prototype vector-based neural networks are able to perform cluster and discrimination analysis on complex physiological signals during drowsiness, like EEG, eye movements and pupil diameter dynamic. As already shown by other authors [20, 21], discrete Fourier transform is an advantageous method for preprocessing the pupil diameter signal. However, an analysis by neural networks does not necessarily need a reduction of features to spectral bands. Several authors have reported large interindividual differences in papillary measurements [6-10, 20-22]. In such cases, neural networks are recommended over the often-used analysis of variance, correlation analysis or student t-tests because neural networks are not based on any assumption of the probability density function. They are model-free methods and are restricted to representative data sets and to the existence of compact regions in feature space only. As shown earlier, a discrimination of wake-sleep transitions is also possible using other types of neural networks [23].

## References

[1] Dinges, D. F.; An Overview of Sleepiness and Accidents; Journal of Sleep Research, Vol 4. Suppl.2. 1995. 4-14.

[2] Horne, J.; Reyner, L.; Sleep-related vehicle accidents; British Medical J, 310, 1995, 565-567.

[3] Santamaria, J.; Chiappa, K.H.; The EEG of Drowsiness in Normal Adults; J Clin Neurol, 4 (4), 1987, 327-382.

[4] Kuhlo, W.; Lehmann, D.; Das Einschlaf-erleben und seine neurophysio-logischen Korrelate; Arch Psychiat Z ges Neurol, 205, 1964, 687-716 (in German).

[5] Maulsby, R.L.; Kellaway, P.; Graham, M. Frost, J.D.Jr; Proler, M.L.; Low, M.D.; North, R.R.; The normative electroencephalographic data reference library; Final Report, Contract NASA 9-1200, National Aeronautics and Space Administration, 1968.

[6] Hyoki, K. et al.; Quantitative electro-oculography and electroencephalography as indices of alertness; Electroenc. Clin. Neurophysiol., 106, 3, 1998, 213-219.

[7] McPartland, R.J.; Kupfer, D.; Computerized measures of electro-oculographic activation during sleep; Int J Biomed Comput, 9, 1979, 409-419.

[8] Ogilvie, R.D.; Mc, D.D.M.; Stone, S.N.; Wilkinson, R.T.; Eye movements and the detection of sleep onset; Psychophysiology, 25, 1988, 81-91.

[9] Schmidt, D.; Abel, L.A.; Dell'Osso, L.F.; Dardoff, R.B.; Saccadic Velocity Characteristics: Intrinsic Variability and Fatigue; Avitation, Space, and Environmental Medicine, 1979, 393-395.

[10] Saito, S.; Does fatique exist in a quantitative measurement of eye movements?; Ergonomics, 35, 1992, 607-615.

[11] Sommer, D.; Golz, M.; Clustering of EEG-segments using hierarchical agglomerative methods and self-organizing maps; in: Dorffner, G.; Bischof, H.; Hornik, K. (eds.): Artificial Neural Networks - ICANN 2001, Berlin, Springer, 2001, 642-649.

[12] Kohonen, T.; Self-organized formation of topologically correct feature maps; Biol Cybern, 43, 1982, 59-69.

[13] Kohonen, T.; Self-Organizing Maps; 3rd edition, Springer, Berlin, 2000.

[14] Fritzke, B.; Growing Cell Structures - a self-organizing network for unsupervised and supervised learning; Neural Networks, 7(9), 1994, 1441-1460.

[15] Villmann, T.; Der, R.; Herrmann, M.; Martinetz, T.M.; Topology Preservation in Self-Organizing Feature Maps: Exact Definition and Measurement; IEEE Trans, Neural Networks 8(2), 1997, 256-266.

[16] Ultsch, A.; Halmans, G.; Data Normalization with Self-Organizing Feature Maps. Int Conf Neural Networks (IJNN-91), Seattle, 1991, I403-I406.

[17] Costa, J.A.F.; Netto, M.L.A.; Estimating the Number of Clusters in Multivariate Data by Self-Organizing Maps; Int. J Neural Systems, 9 (3), 1999, 195-202.

[18] Bauer, H.U.; Pawelzik, K.R.; Quantifying the neighborhood preservation of Self-Organizing Feature Maps; IEEE Trans, Neural Networks, 3 (4), 1992, 570-579.

[19] Golz, M.; Sommer, D.; Lembcke, T.; Kurella, B.; Classification of the pre-stimulus-EEG of k-complexes using competitive neural networks; Proc. 6th Europ. Congress on Intelligent Techniques and Soft Computing - EUFIT'98, Mainz, Aachen, Germany, Vol. 3, 1767-71.

[20] McLaren, J.; Erie, J.C.; Brubaker, R.F.; Computerized analysis of pupillograms in studies of alertness; Investigative Ophthalmology & Visual Science 33, 1992, 671-676.

[21] Grünberger, J., Linzmayer, L., Grünberger, M.; Saletu, B.; Eine neue Methode zur Messung der zentralen Aktivierung: Fourieranalyse der Pupillenoszillationen bei depressiven Patienten; Wien Klin Wochenschr 106, 1994, 164-170 (in German)

[22] Morad, Y.; Lemberg, H.; Yofe, N.; Dagan, Y.; Pupillography as an objective indicator of fatigue; Current Eye Research 21, 2000, 535-542.

[23] Trutschel, U.; Guttkuhn, R.; Ramsthaler, C.; Golz, M.; Moore-Ede, M.; Automatic detection of microsleep events using a neuro-fuzzy hybrid system; Proc. 6th Europ. Congress on Intelligent Techniques and Soft Computing - EUFIT'98. Mainz, Aachen, Germany, Vol. 3, 1762-1766.